JOURNAL OF THE KOREAN ASTRONOMICAL SOCIETY
38: 211 ~ 214, 2005

CHANDRA SPECTROSCOPY OF SUPERNOVA REMNANT 3C 391

YANG CHEN[1], YANG SU[1], PATRICK O. SLANE[2], AND Q. DANIEL WANG[3]
[1]Department of Astronomy, Nanjing University, Nanjing 210093, P.R.China
[2]Harvard-Smithsonian Center for Astrophysics, Cambridge, MA 02138, USA
[3]Department of Astronomy, B619E-LGRT, University of Massachusetts, Amherst, MA01003, USA
(Received February 1, 2005; Accepted March 15, 2005)

ABSTRACT

We performed a spatially resolved spectroscopic study of the thermal composite supernova remnant 3C 391 by the *Chandra* observation. Broad- and narrow-band X-ray images show a southeast-northwest elongated morphology and unveil a highly clumpy structure of the remnant. The spectral analysis for the small-scale features indicates normal metal abundance and uniform temperature for the interior gas. The properties of the hot gas are largely in agreement with the cloudlet evaporation model as a main mechanism for the "thermal composite" X-ray appearance, though radiative rim and thermal conduction may also be effective. An unresolved X-ray source, with a power-law spectrum, is observed on the northwest border. The equivalent width images reveal a faint finger-like protrusion in Si and S lines out of the southwest radio border.

Key words : radiation mechanisms: thermal — supernova remnants: individual: 3C 391 (G31.9+0.0) — X-rays: ISM

I. INTRODUCTION

Supernova remnants (SNRs) with shell-like radio emission and centrally brightened thermal X-rays have now been classified as a category called "thermal composite" or "mixed morphology" SNRs (Jones et al. 1998; Rho & Petre 1998). Many of them are found to interact with adjacent molecular clouds, characterized by the hydroxyl radical maser emission (Green et al. 1997, Yusef-Zadeh et al. 2003). 3C 391 (G31.9+0.0), with irregular morphology, is one of the members of thermal composite SNRs (e.g. Chen & Slane 2001). The physical nature of the internal thermal X-ray emission seen in the thermal composite remnants is still unclear. Here we briefly report our spatially resolved spectroscopic study of 3C 391 based on *Chandra* X-ray observation.

II. DATA ANALYSIS

We observed SNR 3C 391 with the Advanced CCD Imaging Spectrometer (ACIS) on board the *Chandra* X-ray observatory on 2002 August 3. The level 1 raw event data were reprocessed to generate a level 2 event file using the CIAO software package (version 2.3), resulting a net 60.7 ks exposure.

(a) Images

We show the broad-band (0.3-7 keV) diffuse X-ray map in Fig. 1. The equivalent width (EW) maps (i.e., the line-to-continuum ratio maps) for Mg, Si, and S are shown in Fig. 2.

These X-ray images display the southeast-northwest elongated morphology, revealing a highly clumpy structure of the remnant, with clumps or knots located in both the southeast and northwest parts. Several remarkable, very bright knotty features appear on the east and southeast border (regions #1 and #2) of 3C 391. These bright knots on the border may be small clouds that have recently been shocked by the supernova blast wave. A bright enhancement is peaked near the northwest border (region #3). A complex mixture of knots is seen in the southeastern part of the remnant interior, including at least four bright enhancements indicated as regions #6, #7, #8, and #9.

In Fig.1, arc- or shell-like structures are seen along the northeastern and northern rim (regions #10 and #11). An X-ray brightened slab at the west rim appears to be very close to (just slightly behind) the radio peak emission (region #12), and may be related to a small dense region there. On the southwest, faint diffuse emission seems to extend out of the radio border. On the corresponding location in the EW images of Si and S lines (Figs.2b and 2c) there is a finger-like feature protruding radially out of the radio border.

(b) Spectra

After the point-like sources were removed from the data, X-ray spectra were extracted from 17 defined regions (shown in Fig.1). Most of the small-scale regions are chosen to include the small features of X-ray enhancement such as the knots and the faint shell like structures. The distinct line features, Mg Heα ($\sim$ 1.35 keV), Si Heα ($\sim$ 1.85 keV), and S Heα ($\sim$

Proceedings of *the 6th East Asian Meeting of Astronomy*, held at Seoul National University, Korea, from October 18-22, 2004.

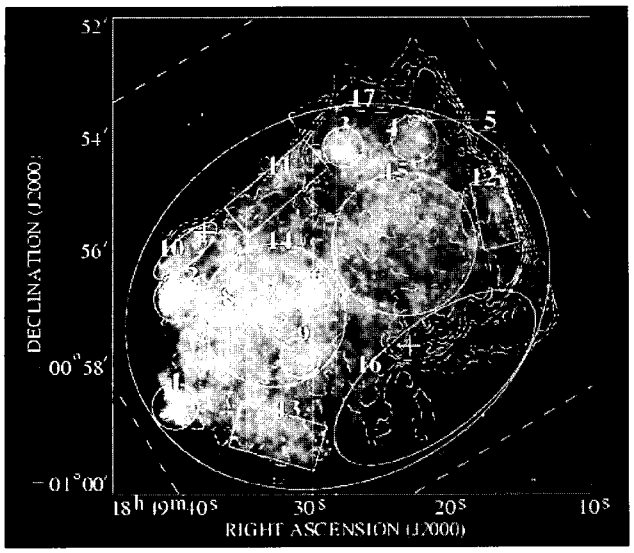

Fig. 1.— Smoothed diffuse emission from SNR 3C 391 in the broad band 0.3-7.0 keV (with count-to-noise ratio of 6). The gray image is logarithmically scaled in the range (1.19–331.85)$\times 10^{-2}$ ct s^{-1} arcmin^{-2}. The location of the sources removed from the data before the smoothing are marked by "×" signs. All the regions used for spectral analysis are indicated with numerical labels. The overlaid 1.5 GHz radio contours are at 1.5, 4.5, 13.6, 28.8, and 50×10^{-3} Jy beam^{-1} (Moffett & Reynolds 1994). The two plus signs denote the OH maser points (Frail et al. 1996). The white dashed lines denote the border of the S3 chip.

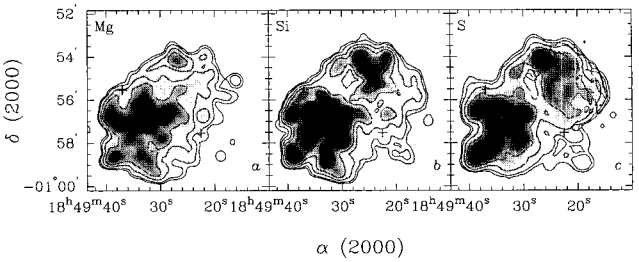

Fig. 2.— EW images of Mg, Si, and S lines. The Mg and Si (S) images are extracted with 4" (8") pixels and smoothed by a Gaussian with $\sigma = 12$" (16"). The seven levels of solid contours are plotted with square-root intensity scales between the maximum and the 3% maximum brightness. The two plus signs in each panel denote the OH maser points.

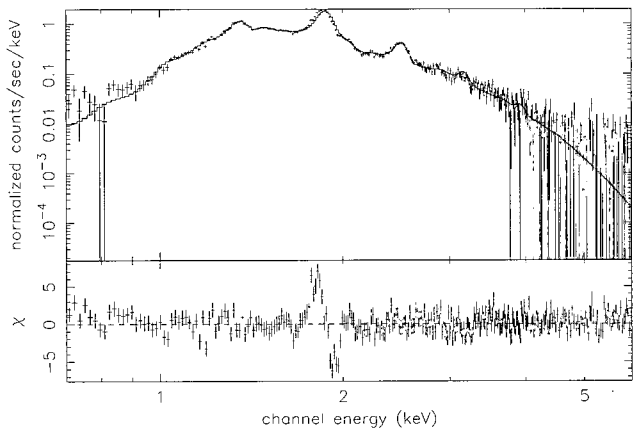

Fig. 3.— *Chandra* ACIS spectra of the entire remnant of 3C 391 fitted with the VNEI model.

2.46 keV) in the spectra (see Fig.3) indicate the thermal origin of the diffuse gas. We find that the spectra of the diffuse gas can be best described by the VNEI model with the correction of interstellar absorption. The spectral fit results are tabulated in the Table.

The absorption column density is found to generally increase across the remnant from southeast to northwest, consistent with the existence of a molecular cloud to the northwest (Wilner et al. 1998). The spectral fits show that the diffuse emission from various regions have ionization parameters ($n_e t$) close to or higher than 10^{12} cm^{-3} s. This implies that the hot plasma in the SNR is very close to, or is basically in, the ionization equilibrium. The spectral fits also show that the diffuse emission from various regions can be well fitted with solar abundances or abundances very close to solar values. The temperature of the gas interior to the SNR is generally ~0.5-0.6 keV, with only small fluctuations. The gas density of each defined region was roughly estimated (as also listed in the Table). Apart from the compact knots on the southeast and eastern boundary (with a density $10\text{–}20 f^{-1/2} d_8^{-1/2}$ cm^{-3}), most of the bright knots have a gas density $\sim 5\text{–}7 f^{-1/2} d_8^{-1/2}$ cm^{-3} and most of the regions along the remnant border have a density $\sim 1\text{–}3 f^{-1/2} d_8^{-1/2}$ cm^{-3} (where $d_8 = d/8$ kpc denotes the distance and f is the filling factor of the X-ray emitting gas). The X-ray luminosity in 0.5–10 keV of the remnant is $\sim 3.5 \times 10^{36} d_8^2$ ergs s^{-1}.

III. THE COMPOSITE APPEARANCE

At least four candidate scenarios up to date compete to account for centrally-brightened X-ray morphology. The first scenario is radiative cooling of the rim gas. Under this hypothesis, the gas at the rim has been cooled down in the radiative stage, with a temperature so low that its X-ray emission is very weak, while the gas in the inner volume is still hot enough to emit strong X-rays (e.g. Rho & Petre 1998). The second mechanism invokes thermal conduction. It is suggested that thermal conduction in the remnant can prevent formation of the very tenuous, hot gas in the inner part and therefore change the interior structure from the standard Sedov solution, resulting in a non-negligible density and luminous X-ray in the interior (as observed in, especially, the radiative stage) (Cox et al. 1999). The third scenario is cloudlet evaporation in the SNR interior. When an SNR expands in an inhomogeneous interstellar medium (ISM) whose mass is

TABLE 1.
VNEI FITTING RESULTS WITH THE 90% CONFIDENCE RANGES

regions	χ^2/d.o.f.	$N_{\rm H}$ (10^{22} cm^{-2})	kT_x (keV)	$n_e t$ (10^{11} cm^{-3} s)
1	90.5/65	2.8 ± 0.1	$0.67^{+0.02}_{-0.04}$	> 200
2	87.0/79	2.7 ± 0.1	$0.58^{+0.06}_{-0.05}$	$5.1^{+4.6}_{-1.3}$
3	68.8/48	3.4 ± 0.2	$0.56^{+0.06}_{-0.09}$	> 6.4
4[a]	108.9/79	$4.1^{+0.3}_{-0.2}$	$0.62^{+0.04}_{-0.05}$	> 30
6	65.2/58	$2.7^{+0.2}_{-0.1}$	$0.56^{+0.08}_{-0.06}$	$5.0^{+3.8}_{-2.1}$
7	57.8/58	$3.0^{+0.1}_{-0.2}$	$0.54^{+0.05}_{-0.06}$	> 5.5
8	72.4/52	$2.9^{+0.2}_{-0.1}$	$0.63^{+0.08}_{-0.07}$	> 3.4
9	58.2/43	2.9 ± 0.2	$0.63^{+0.07}_{-0.11}$	> 2.7
10	44.2/44	$3.0^{+0.2}_{-0.1}$	$0.79^{+0.14}_{-0.10}$	$3.1^{+3.6}_{-1.4}$
11	96.9/72	2.8 ± 0.1	$0.59^{+0.06}_{-0.04}$	> 3.8
12	49.8/32	$3.7^{+0.6}_{-0.4}$	$0.58^{+0.11}_{-0.12}$	> 265
13	107.0/82	$3.0^{+0.2}_{-0.1}$	$0.46^{+0.04}_{-0.03}$	> 106
14[a]	273.6/180	2.9 ± 0.1	0.55 ± 0.02	> 9.0
15[a]	237.8/163	3.5 ± 0.1	$0.54^{+0.02}_{-0.01}$	> 23
16[a]	156.3/127	3.2 ± 0.2	$0.53^{+0.04}_{-0.06}$	> 239
17[a]	710.5/296	3.1 ± 0.1	0.56 ± 0.01	> 12.8

a: Making abundances of Mg, Si, and S free parameters apparently improves the fit. For region #4, [Mg/H] = $1.23^{+0.69}_{-0.44}$, [Si/H] = $0.66^{+0.19}_{-0.15}$, [S/H] = $0.51^{+0.22}_{-0.20}$; for region #14, [Mg/H] = $1.12^{+0.13}_{-0.09}$, [Si/H] = $0.87^{+0.08}_{-0.05}$, [S/H] = $0.80^{+0.13}_{-0.09}$; for region #15, [Mg/H] = $0.92^{+0.14}_{-0.13}$, [Si/H] = 0.53 ± 0.05, [S/H] = $0.64^{+0.12}_{-0.11}$; for region #16, [Mg/H] = $0.93^{+0.28}_{-0.26}$, [Si/H] = $0.54^{+0.12}_{-0.11}$, [S/H] = $0.54^{+0.24}_{-0.21}$; and for region #17, [Mg/H] = $0.97^{+0.07}_{-0.05}$, [Si/H] = 0.70 ± 0.03, [S/H] = $0.71^{+0.06}_{-0.05}$.

mostly contained in small clouds, the clouds engulfed by the blast wave can be evaporated to gradually increase the density of the interior gas; consequently, the SNR appears internally X-ray brightened (White & Long 1991). The fourth suggestion is that the mixed morphology is a projection effect. For shell-like SNRs that evolve in a density gradient such as at the edge of a molecular cloud, if the line of sight is essentially aligned with the density gradient as well as the magnetic field, the SNRs will appear as thermal composites (Petruk 2001).

We thus briefly compare the four mechanisms with the properties found from our spatially-resolved spectral analysis.

(1) *Projection Effect* The molecular cloud is located in the northwest but the X-ray emission is enhanced not only in the northwestern half, but also in the southeastern half. Additionally, the variation of the hydrogen column density across the remnant implies that the density gradient of the ambient medium seems to be close to the projection plane. Therefore, the projection effect does not match the observational properties. (2) *Radiative Rim* The filamentary near-infrared [Fe II] and the mid-infrared 12-18 μm [Ne II] and [Ne III] emission along the northwestern radio shell provide some evidence for a radiative cooling at the rim (Reach, Rho, & Jarrett 2002). Along the northwestern border, the shell formation time is $t_{\rm shell} \approx 3.8 \times 10^3 E_{51}^{3/14}$ yr, comparable to remnant's age $t = (2/5)(r_s/v_s) \sim 4 \times 10^3$ yr. However the X-ray emission along the border (e.g. regions #10, #11, #12, and #16), which arises from hot gas ($\sim 7 \times 10^6$ K), indicates that a considerable amount of gas at the blast shock has not yet suffered significant radiative cooling. Additionally, the rim cooling mechanism can not explain what the central bright clumpy emission is. (3) *Thermal Conduction* For 3C 391, the thermal conduction scenario is favored by the radiative filaments along the northwestern border and the high ionization timescale implicative of relatively little newly shocked material. The conduction timescale $t_{\rm cond} \sim 5.2 \times 10^3 (\ell/2.3\,{\rm pc})^2$ yr for the spatial scale ℓ of order the separation between clumps (typified by $1' \sim 2.3$ pc) is comparable to the remnant's age and hence implies a role of conduction in smoothing the interior temperature profile. However, the thermal conduction scenario asks for a decrease of temperature and an increase of gas density with remnant radius. This predicted behavior is inconsistent with the uniform distribution of the gas temperature and density. (4) *Cloudlet Evaporation* The relatively uniform distribution of temperature (even with slightly lower values at the center) is actually expected by the White & Long (1991) cloudlet evaporation model for model parameters $\tau \rightarrow \infty$ and $C/\tau \gtrsim 3$, where τ is the ratio of the cloud evaporation timescale to the SNR's age and C is the ratio of the mass in the cloudlets to the mass of ICM. The ratio between the mean density ($\sim 2 f^{-1/2} d_8^{-1/2}$ cm^{-3}) and the density along the border (~ 1–$3 f^{-1/2} d_8^{-1/2}$ cm^{-3}) is basically consistent with that predicted in the evaporation model. In fact, the highly clumpy structure unveiled in this observation lends support to the conjecture that the ambient molecular cloud is inhomogeneous. A combination of very dense clumps and moderately dense gas are directly observed in the millimeter molecular lines (Reach & Rho 1999). The cloudlets engulfed by the supernova blast wave can act as a large reservoir of interior gas by gradual evaporation. This could also explain why the interior gas density is much lower than that of the ambient cloud gas ($\sim$ 30-100 cm^{-3}). With this model, the supernova explosion energy is $E \sim 0.3$–$1.4 \times 10^{51} d_8^3 (n_0/0.3\,{\rm cm}^{-3})$ ergs. The main difficulty with the model is the high ionization age ($> 10^{12}$ s) in some regions (e.g. region #1) opposed to the low age of the newly evaporated gas.

IV. THE UNRESOLVED SOURCE

The association of 3C 391 with a dense molecular cloud makes it possible that 3C 391 is the interstellar remnant of the supernova explosion of a massive star, which may also leave behind a compact star as a result of gravitational core collapse. We locate numerous point-like sources within the boundary (and even near the center) of the remnant. However, spectral analysis for these sources cannot be carried out because of the small number of counts.

A bright unresolved source (within region #5) ap-

pears near the northwest rim. The spectrum of this source extracted from region #5 is better described with a power law than with a bremsstrahlung or blackbody. The hydrogen column density obtained ($2.6^{+1.4}_{-1.0} \times 10^{22}\,\mathrm{cm}^{-2}$) is similar to those of other portions of this remnant. If this source is at the distance of 3C 391, its unabsorbed X-ray luminosity is $\sim 7.0 \times 10^{32} d_8\,\mathrm{ergs\,s}^{-1}$. If the association with the gaseous remnant is true, the stellar remnant may have moved away from its explosion site with a displacement velocity $\sim 1100\,\mathrm{km\,s}^{-1}$.

V. THE SOUTHWEST PROTRUSION

The finger-like protruding feature on the southwest seen in the Si and S EW maps (Fig. 2) looks somewhat similar to the apparent protrusion in Si and S lines recently revealed on the northeastern border of SNR Cas A (Hwang et al. 2000). The protruding feature of Cas A has been explained as one of the jets of ejecta extending outside of the blast shock (Hwang et al. 2000, 2004). The small number of counts collected for the feature in 3C 391 makes it difficult to determine the metal abundances. If the jet-like structure in 3C 391 is true, it might be yielded by an asymmetric supernova explosion of a massive core-collapse progenitor star and such an asymmetric structure was not erased by the low mass hydrogen envelope at explosion as in the case of 3C 391 (Hwang et al. 2004).

VI. CONCLUSION

We observed the thermal composite SNR 3C 391 using *Chandra* X-ray observatory and carried out a spatially resolved spectroscopic study of the SNR. The main results are summarized as follows.

1. Broad- and narrow-band X-ray images show a southeast-northwest elongated morphology and unveil a highly clumpy structure of the remnant. The spectral analysis for the small-scale features indicates normal metal abundance and uniform temperature for the interior gas.
2. The physical properties of the hot gas are essentially in agreement with the cloudlet evaporation model as a main mechanism for the "thermal composite" X-ray appearance, though radiative rim and thermal conduction may also be effective.
3. An unresolved X-ray source is observed on the northwest border, whose spectrum is best fitted with a power law.
4. The equivalent width images reveal a faint finger-like protrusion in Si and S lines out of the southwest radio border.

ACKNOWLEDGEMENTS

This work is supported by NSFC grants 10073003 & 10221001, CMST grant NKBRSF-G19990754, NASA contract NAS8-39073, and NASA grants GO2-3081X & NAG5-8935.

REFERENCES

Chen, Y., & Slane, P. O., 2001, *ASCA* Observations of the Thermal Composite Supernova Remnant 3C 391, ApJ, 563, 202

Cox, D. P., Shelton, R. L., Maciejewski, W., Smith, R. K., Plewa, T., Pawl, A., & Rózyczka, M., 1999, ApJ, 524, 179

Frail, D. A., Goss, W. M., Reynoso, E.M., Giacani, E. B., Green, A. J., & Otrupcek, R., 1996, AJ, 111, 1651

Green, A. J., Frail, D. A., Goss, W. M., & Otrupcek, R. 1997, AJ, 114, 2058

Jones, T. W. et al., 1998, PASP, 110, 125

Hwang, U., Holt, S. S., & Petre, R., 2000, ApJ, 537, L119

Hwang, U. et al., 2004, ApJ, 615, L117

Moffett, D. A., & Reynolds, S. P., 1994, ApJ, 425, 668

Petruk, O., 2001, A&A, 371, 267

Reach, W. T., & Rho, J. H., 1999, ApJ, 511, 836

Reach, W. T., Rho, J. H., & Jarrett, T. H., 2002, ApJ, 564, 302

Rho, J. H., & Petre, R., 1998, ApJ, 503, L167

White, R. L., & Long, K. S., 1991, ApJ, 373, 543

Wilner, D. J., Reynolds, S. P., & Moffett, D. A., 1998, ApJ, 115, 247

Yusef-Zadeh, F., Wardle, M., Rho, J., & Sakano, M., 2003, ApJ, 585, 319